detonationFoam: An open-source solver for simulation of gaseous detonation based on OpenFOAM

Jie Sun[a], Yiqing Wang[a], Baolin Tian[b,a], Zheng Chen[a,c*]

[a]HEDPS, Center for Applied Physics and Technology, College of Engineering, Peking University, Beijing 100871, China

[b]LCP, Institute of Applied Physics and Computational Mathematics, Beijing 100094, China

[c]State Key Laboratory of Turbulence and Complex Systems, Peking University, Beijing 100094, China

Abstract

Detonation has promising applications in advanced propulsion systems, and numerical simulation is widely used to gain insights into the complex interaction between the hydrodynamic flow and chemical reactions involved in detonation. In this work, detonationFoam, an open-source solver for accurate and efficient simulation of compressible reactive flow and detonation is developed based on OpenFOAM. detonationFoam can simulate compressible, multi-component, reactive flow and it can accurately evaluate the detailed transport coefficients using the mixture-averaged transport model. Compared to rhoCentralFoam, the improved HLLC-P approximate Riemann solver is used in detonationFoam and it helps to accurately resolve shock waves appearing in detonation. Besides, the adaptive mesh refinement and dynamic load balancing algorithms are used in detonationFoam, which greatly improves the computational efficiency. Validation tests including homogenous ignition, unsteady diffusion, shock tube problem, premixed flame, planar detonation, double Mach reflection, detonation cellular structure and oblique detonation wave are conducted. These tests demonstrate that detonationFoam can be used to accurately and efficiently to simulate the compressible, multi-component reactive flow and detonation processes.

***Keywords**:* Detonation; Simulation; Compressible reactive flow; OpenFOAM.

* Corresponding author. E-mail: cz@pku.edu.cn (Z. Chen)

Program summary

Program Title: detonationFoam

CPC Library link to program files: (to be added by Technical Editor)

Developer's repository link: (to be added by the author)

Code Ocean capsule: (to be added by Technical Editor)

Licensing provisions: GPLv3

Programming language: C++

Nature of problem: Gaseous detonation involves different length scales and complicated chemistry. To accurately and efficiently simulate the gaseous detonation, adaptive mesh refinement needs to be conducted and detailed chemistry should be considered. Besides, the severe load imbalance caused by the chemical source term evaluation may greatly reduce the computation efficiency.

Solution method: An open-source solver, detonationFoam is developed based on OpenFOAM. The species equations considering detailed chemistry are solved in detonationFoam and thereby detonation in a compressible, multi-component, reactive flow can be simulated. The adaptive mesh refinement technique and the dynamic load balancing algorithm are incorporated into detonationFoam. It is demonstrated that detonationFoam can accurately and efficiently simulate gaseous detonation.

1. Introduction

Detonation has received increasing interest in recent years since it can achieve higher thermal efficiency and faster heat release rate than deflagration and thereby has promising applications in advanced propulsion systems [1-5]. Since it is very difficult to measure the transient detonation process in experiments, numerical simulation is popularly used to gain insights into the complex interaction between the hydrodynamic flow and chemical reactions involved in detonation [6-10]. Though several codes have been developed by different groups to simulate different detonation processes, they are not open-source and thereby are not available to all researchers. Therefore, it is necessary to develop an open-source code for detonation simulation in a rigid framework and readily for further extension. This motivates the present study, which aims to develop an open-source solver for accurate and efficient simulation of compressible reactive flow and detonation based on OpenFOAM [11].

OpenFOAM is one of the most popular open-source libraries and has been successfully applied to both non-reactive and reactive flows [12-14]. In the context of simulating low-speed reactive flow (i.e., deflagration), many researchers have developed their solvers based on reactingFoam (e.g., [15-18]). Usually, the simplified molecular transport model used by default in reactingFoam [11] needs to be replaced by detailed model (e.g., mixture-averaged model or multicomponent model [19, 20]) so that flame propagation can be accurately simulated [15-18]. Besides, CVODE [21] is usually incorporated into reactingFoam to solve the stiff ordinary differential equations (ODEs) when detailed kinetic models are considered [17]. After these modifications, deflagration/flame can be accurately simulated using reactingFoam.

Unlike deflagration whose propagation speed is in the order of 1 m/s and thereby can be approximated to be isobaric, detonation propagates supersonically at speeds in the order of 1000 m/s and it consists of a leading shock wave followed by a reaction zone [22]. The inherent disparity of scales involved in detonation requires sufficient resolution both in space and time for the leading shock and the reaction zone, which brings challenges to detonation simulations. In OpenFOAM, the density-based solver,

rhoCentralFoam [11], is developed for high-speed flows with shock waves; and the central-upwind Kurganov and Tadmor (KT) scheme [23] or Kurganov, Noelle and Petrova (KNP) scheme [24] is adopted to capture the shock wave and contact discontinuity. Based on rhoCentralFoam, Marcantoni et al. [25] developed rhoCentralRfFoam to simulate detonation considering governing equations for multi-species and detailed chemistry. They showed that rhoCentralRfFoam can accurately predict the detonation velocity and two-dimensional cellular detonation. After that, several rhoCentralFoam-based solvers have been developed, such as rhoHLLCFoam developed by Liu et al. [26] and RYrhoCentralFoam developed by Huang et al. [27]. In rhoHLLCFoam [26], the Harten-Lax-van-Leer-Contact (HLLC) scheme [28] was used to calculate the convective flux. In RYrhoCentralFoam, Huang et al. [27] incorporated the Lagrangian solver for gas-droplet two-phase flows and thereby it was used to simulate detonation in gas-liquid mixtures [29, 30].

Although the above studies have shown different levels of success in developing rhoCentralFoam-based solvers to simulate detonation, there are still some aspects needing to be improved. First, the Sutherland law is usually used to calculate transport coefficients in detonation solvers. As a result, the multi-species transport process cannot be accurately predicted, and this may lead to large discrepancy for cases (e.g., the deflagration to detonation process) in which the transport process plays an important role. Second, though various techniques have been proposed to reduce the computational cost, they have not been incorporated simultaneously into detonation solvers. As mentioned above, high spatial resolution is required to capture the detonation structure. Since special resolution is required mainly for the region around the detonation front, dynamically adaptive mesh refinement (AMR) is suitable for detonation simulation. However, OpenFOAM only supports AMR for hexahedral cells in 3D [11, 31, 32] which is not appropriate for 2D detonation simulation. Furthermore, when the AMR technique is adopted in conjunction with finite-rate chemistry, the severe load imbalance may greatly reduce the computation efficiency. Specifically, when the computational domain is decomposed and distributed to the different processors, some processors might have much more cells in the reaction zone than

others. Since in the reaction zone the ODEs are stiff, it takes lots of computation time. Therefore, the processor that has the maximum cell number in the reaction zone becomes the bottleneck and other processors have to wait for synchronization. To tackle this issue, Tekgul et al. [33] and Zirwes et al. [34] proposed the dynamic load balancing (DLB) algorithm based on forming groups of processors that share their chemistry workload. The DLB algorithm was successfully used for simulating deflagration processes and the speed-up around 10 was achieved [33]. However, these acceleration techniques, AMR and DLB, have not been simultaneously used in detonation solvers. Besides, the rhoCentralFoam-based detonation solvers mentioned above are not open-source. Though McGough [35] provided an open-source solver, rhoReactingCentralFoam, for detonation simulation, its accuracy was not examined comprehensively and the load imbalance problem was not solved.

Based on the above consideration, this work aims to develop an OpenFOAM-based open-source solver, detonationFoam, which can accurately and efficiently simulate gaseous detonation. The following five implementations are made based on rhoCentralFoam. First, the species equations and finite-rate chemistry model are incorporated to simulate compressible multi-species reactive flow. Second, the mixture-averaged transport model is used to evaluate the multi-species transport properties. Third, the HLLC-P (HLLC with a pressure-control technique) approximate Riemann solver [36, 37] is incorporated to achieve accurate shock wave capturing. Fourth, the AMR technique is incorporated into the solver so that the detonation front and different waves can be accurately and efficiently resolved. Fifth, the DLB algorithm is used to further improve the computational efficiency. The reliability of detonationFoam on modeling different processes including detonation is verified by comparing the typical simulation results with those in the literature. Note that blastFoam [38] has been successfully in the simulation of high-explosive detonation, explosive safety and airblast. BlastFoam can simulate explosion and detonation in multi-phase energetic materials while detonationFoam focus more on simulating gaseous detonation.Nevertheless, blastFoam was not validated in terms of simulating flames and deflagration-to-detonation transition in which multi-species transport is important.

The remainder of this paper is structured as follows. The governing equations and numerical methods are described in Section 2. The reliability and application of the open-source solver detonationFoam is shown in Section 3. Finally, conclusions are drawn in Section 4.

2. Governing equations and numerical methods

2.1 Governing equations

The conservation equations for unsteady, compressible, multi-component reactive flow are solved in detonationFoam. The governing equations [39] for mass, momentum, energy and species are

$$\frac{\partial \rho}{\partial t} + \nabla \cdot (\rho V) = 0 \tag{1}$$

$$\frac{\partial (\rho V)}{\partial t} + \nabla \cdot (\rho VV) = -\nabla P + \nabla \cdot \tau \tag{2}$$

$$\frac{\partial (\rho E)}{\partial t} + \nabla \cdot [(\rho E + P)V] = -\nabla \cdot q + \nabla \cdot (V \cdot \tau) \tag{3}$$

$$\frac{\partial (\rho Y_k)}{\partial t} + \nabla \cdot [\rho (V + V_k^{'}) Y_k] = \omega_k \qquad k = 1, ..., N_S - 1 \tag{4}$$

Here, ρ is the density of the mixture, $V = (u, v, w)$ is the velocity vector, and P is the pressure. Y_k, $V_k^{'}$ and ω_k are respectively the mass fraction, diffusion velocity and production rate of the *k-th* species. N_S is the total number of the species. The viscous stress is

$$\tau = \mu \left[\nabla V + (\nabla V)^T - \frac{2}{3} I (\nabla \cdot V) \right] \tag{5}$$

in which μ is the dynamic viscosity of the mixture and I is the unit tensor.

We assume that the mixture is ideal gas and the equation of state is:

$$P = \frac{\rho R T}{\overline{W}} \tag{6}$$

where T is the temperature, $R = 8.314$ J/(mole·K) is the universal gas constant, and $\overline{W}$ is the mean molar weight of the mixture.

The total energy E and heat flux q in Eq. (3) are [39]

$$q = -\lambda \nabla T + \rho \sum_{k=1}^{N_S} \left(Y_k h_k V_k^{'} \right) \tag{7}$$

$$E = -\frac{P}{\rho} + \frac{V^2}{2} + \sum_{k=1}^{N_S} \left(Y_k h_k \right) \tag{8}$$

where λ is the thermal conductivity of the mixture, and h_k is the enthalpy of the *k-th* species. The thermodynamic properties of each species are evaluated with *JANAF* polynomials [40]. The enthalpy, h_k, and the specific heat capacity at constant pressure, $C_{p,k}$ of the *k-th* species are:

$$\frac{h_k}{RT} = \sum_{n=0}^{4} \frac{a_{n,k} T^n}{n+1} + \frac{a_{n,5}}{T} \tag{9}$$

$$\frac{C_{p,k}}{R} = \sum_{n=0}^{4} a_{n,k} T^n \tag{10}$$

where $a_{n,k}$ with n = 1~5 are the coefficients for the *k-th* species.

The mixture-averaged transport model is added in detonationFoam to calculate the transport properties. Cantera [41] is popularly incorporated into OpenFOAM to evaluate transport coefficients [15, 17, 18]. Here the transport calculation module provided by Dasgupta et al. [16] is modified and incorporated into detonationFoam . The Wilke formula [42, 43] is used to calculate the dynamic viscosity of the mixture:

$$\mu = \sum_{k=1}^{N_S} \frac{X_k \mu_k}{\sum_{j=1}^{N_S} X_j \Phi_{kj}} \tag{11}$$

where X_k is the mole fraction and μ_k is the dynamic viscosity coefficient of the *k-th* species. Φ_{kj} is the dimensionless partition function defined as [43]:

$$\Phi_{kj} = \frac{1}{\sqrt{8}} \left(1 + \frac{W_k}{W_j} \right)^{-\frac{1}{2}} \left[1 + \left(\frac{\mu_k}{\mu_j} \right)^{\frac{1}{2}} \left(\frac{W_j}{W_k} \right)^{\frac{1}{4}} \right]^2 \tag{12}$$

where W_k is the molecular weight of the *k-th* species.

The thermal conductivity of the mixture is obtained from the following formula [44]

$$\lambda = \frac{1}{2}\left(\sum_{k=1}^{N_S} X_k \lambda_k + \frac{1}{\sum_{k=1}^{N_S} \frac{X_k}{\lambda_k}} \right) \tag{13}$$

where λ_k is the thermal conductivity of the *k-th* species.

The diffusion velocity, $V_k^{'}$ in Eq. (4), consists of three parts [45]

$$V_k^{'} = V_{k,Y}^{'} + V_{k,T}^{'} + V_{k,C}^{'} \tag{14}$$

where $V_{k,Y}^{'}$ is the ordinary diffusion velocity and $V_{k,T}^{'}$ is the thermal diffusion velocity. The expressions for $V_{k,Y}^{'}$ and $V_{k,T}^{'}$ are:

$$V_{k,Y}^{'} = -\frac{D_{km}}{X_k}\frac{\partial X_k}{\partial x_i} \tag{15}$$

$$V_{k,T}^{'} = -\frac{D_{km}\Theta_k}{X_k}\frac{1}{T}\frac{\partial T}{\partial x_i} \tag{16}$$

where D_{km} is the mixture-averaged mass diffusion coefficient and Θ_k is the thermal diffusion ratio of the *k-th* species.

The correction velocity, $V_{k,C}^{'}$, is introduced to ensure the compatibility between the species mass conservation and the total mass conservation [39]. It is determined according to the following requirement:

$$\sum_{k=1}^{N_S} \left(\rho Y_k V_k^{'} \right) = 0 \tag{17}$$

In detonationFoam, the detailed kinetic model can be considered. For a kinetic model containing N_S species, the N_R elementary reactions can be written as [19]

$$\sum_{k=1}^{N_S} (\nu_{k,j}^{'} M_k) \underset{K_{b,j}}{\overset{K_{f,j}}{\Leftrightarrow}} \sum_{k=1}^{N_S} (\nu_{k,j}^{''} M_k) \qquad j = 1, \ldots, N_R \tag{18}$$

Here M_k represents the molecular formula for the *k-th* species. $\nu_{k,j}^{'}$ and $\nu_{k,j}^{''}$ are the stoichiometric coefficients of the *k-th* species in the *j-th* elementary reaction. $K_{f,j}$ and $K_{b,j}$ respectively represent the forward and backward reaction rate constants of the *j-th* elementary reaction. The production rate of the *k-th* species can be expressed as [19]

$$\omega_k = W_k \sum_{j=1}^{N_R} [(\nu_{k,j}^{''} - \nu_{k,j}^{'})(K_{f,j} \prod_{k=1}^{N_S} C_k^{\nu_{k,j}^{'}} - K_{b,j} \prod_{k=1}^{N_S} C_k^{\nu_{k,j}^{''}})] \tag{19}$$

where C_k is the molar concentration of the *k-th* species. The reaction rate constant, $K_{f,j}$, can be written in the Arrhenius Law [19] as

$$K_{f,j} = A_j T^{\beta_j} \exp(-\frac{E_{a,j}}{RT}) \tag{20}$$

Here A_j, β_j and $E_{a,j}$ are respectively the pre-exponential factor, temperature exponent and activation energy of the *j-th* forward reaction. The backward reaction rate, $K_{b,j}$, can be evaluated based on $K_{f,j}$ and the equilibrium constant of the *j-th* elementary reaction [19].

2.2 Numerical methods

2.2.1 Numerical schemes

Since detonationFoam is developed based on OpenFOAM, the numerical schemes provided by OpenFOAM are directly used. The second order MUSCL scheme [46] with HLLC-P approximate Riemann solver [36] is used to calculate the convective fluxes, and the second-order central difference scheme is used for diffusion fluxes. Operator splitting fractional-step procedure [18] is used to separate the time evolution of the stiff reaction term from that of the convection and diffusion terms. In the time advance of the non-reactive flow, the first order implicit Euler scheme is used. Though the second-order scheme such as the backward scheme and Crank-Nicolson scheme can also be used, it has little influence on the results due to the very small time step in the order of 10^{-9} s. The seulex ODE solver [47] has been proved to be robust and efficient for stiff system by employing an extrapolation algorithm, based on the linearly implicit Euler method with step size control and order selection. Therefore, it is adopted here to solve the ODEs describing the chemical reactions.

To accurately capture shock waves and contact discontinuities, the HLLC-P approximate Riemann solver [36] is used. A pressure dissipative term, Φ_P, is added into the flux of the HLLC Riemann solver [28], Φ_{HLLC}, and thereby the convective flux in the HLLC-P Riemann solver becomes [36, 48]:

$$\Phi_{HLLC-P} = \Phi_{HLLC} + \Phi_P \tag{21}$$

where

$$\Phi_{HLLC}=\begin{cases}F_L & 0<S_L\\ F_L+S_L(U_L^*-U_L) & S_L\le 0<S^*\\ F_R+S_R(U_R^*-U_R) & S^*<0\le S_R\\ F_R & 0>S_R\end{cases} \tag{22}$$

Here U_L, U_L^*, U_R^*, U_R are the conserved variables in regions #1, #2, #3 and #4 as shown in Fig. 1. F_L and F_R are respectively the left and right reconstructed fluxes. The propagation speed of the contact discontinuity is denoted as S^*. S_L and S_R are the propagation speeds of the left and right traveling waves, respectively.

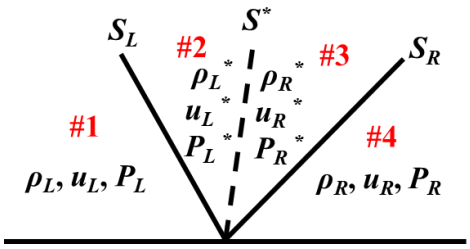

Fig. 1. Schematic of wave structures of the HLLC approximate Riemann solver.

In Eq. (21), Φ_P is the pressure dissipative term which provides damping to suppress oscillations and is defined as [36]

$$\Phi_p=(f-1)\frac{S_L S_R}{S_R-S_L}\frac{1}{1+|\bar{M}|}\frac{|P_R-P_L|}{\bar{c}^2}\left(1,\bar{u},\bar{v},\frac{1}{2}\bar{q}^2\right)^T \tag{23}$$

where $\bar{M}$, $\bar{c}$, $\bar{u}$, $\bar{v}$ and $\bar{q}$ are respectively the Mach number, speed of sound, velocity components and the normal velocity evaluated by Roe averaged method at the interface [36]. f is the function of P_L and P_R, which is defined as [36]

$$\begin{cases} f=\left[\min\left(f_{P,(I,J+1/2)},f_{P,(I-1/2,J)},f_{P,(I-1/2,J+1)},f_{P,(I+1/2,J)},f_{P,(I+1/2,J+1)}\right)\right]^3\\ f_P=\min\left(\dfrac{P_R}{P_L},\dfrac{P_L}{P_R}\right)\end{cases} \tag{24}$$

Here the subscripts, (I, J+1/2), (I-1/2, J), (I-1/2, J+1), (I+1/2, J) and (I+1/2, J+1), are mesh nodes as the reference [36] describes.

2.2.2 Adaptive mesh refinement

As stated before, adaptive mesh refinement helps to efficiently resolve the propagating detonation. Therefore, AMR is used in detonationFoam. Following the work of Baniabedalruhman [31], the AMR library provided by OpenFOAM is modified and incorporated into detonationFoam for 2D simulations while the original AMR library is suitable only for 3D simulations.

Here the 2D case is used as the example to describe the mesh refinement/ coarsening process. In AMR, mesh refinement and coarsening criteria should be specified before the simulation. As an example, mesh refinement/ coarsening can be conducted based on the magnitude of local density gradient $|\nabla\rho|$. When $|\nabla\rho|$ at the face center (red points in Fig. 2) is larger than a threshold value, $|\nabla\rho|_R$, mesh refinement should be conducted. Then, the four edges of the cell are divided equally by the blue points shown in Fig. 2. Subsequently, the cell is divided into four adjacent sub-cells. Then all values are mapped from the original mesh to the new refined mesh. Mapping of field values is implemented in a straightforward and conservative manner[32]. For the refinement step, sub-cells receive the cell-centered value of the parent cell. For the coarsening step, the average values of sub-cells are set on the parent cell. After the refinement is done, the fluxes are corrected using the mapped values. Similarly, when $|\nabla\rho|$ is smaller than another threshold value, $|\nabla\rho|_C$ (which is smaller than $|\nabla\rho|_R$), coarsening should be conducted to restore the mesh from the refinement state to the original state. The above AMR process in detonationFoam is depicted in Table 1.

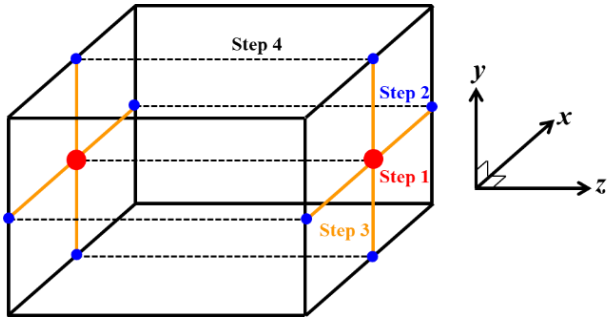

Fig. 2 Schematic of the steps during the 2D mesh refinement process.

Table 1 Pseudo-code of the mesh refinement/coarsening process.

Step. 1: Calculate the magnitude of local density gradient, $\|\nabla\rho\|$.
Step. 2: Iterate through cells and compare the magnitude between $\|\nabla\rho\|$ on each *cell* with the refinement criterion. Mesh refinement and coarsening are conducted as: *For the i-th cell in all cells* *If* ($\|\nabla\rho\|_i > \|\nabla\rho\|_R$) *If the i-th cell has not reached the maximum cell level* *refining the i-th cell* *endif* *else if* ($\|\nabla\rho\|_i < \|\nabla\rho\|_C$) *If the i-th cell has been refined* *coarsening the i-th cell* *endif* *endif* *End*
Step. 3: Update the states by mapping the data from the original mesh to the updated mesh.
Step. 4: Calculate the fluxes using the updated values.

2.2.3 Dynamic load balancing

As mentioned above, the DLB algorithm helps to effectively balance the CPU-calculation time for solving the stiff ODEs. It is usually used in the parallel simulation of reactive flow considering detailed kinetic models, which might consist of a large number of species and elementary reactions. The open-source DLB algorithm, DLBFoam, developed by Tekgul et al. [33] is incorporated into detonationFoam.

The pseudo-code of the DLB algorithm used in detonationFoam is depicted in Table 2. When N processors are used, the cost of each processor at time t is counted and signed as $[l_1, l_2, \ldots, l_N]$. The total cost, L, and the average cost, $\overline{L}$, are defined as

$$L = \sum_{k=1}^{N} l_k \tag{25}$$

$$\bar{L} = L / N \tag{26}$$

If $l_k < \bar{L}$, then the k-th processor is designated as the receiver process. On the other hand, the sender processors are those with $l_k > \bar{L}$. The sender processors send their excess load to receiver processors so that the cost for each processor is close to $\bar{L}$. Then the stiff ODEs are solved using the new distributed load in each processor and the updated value is sent back to the original processor.

Table 2 Pseudo-code of the dynamic load balancing algorithm.

Step. 1: Count the total load of chemical calculation of each processor, [l_1, l_2, ..., l_N], at the last time. (N is the number of the processors)
Step. 2: Calculate the total load. $$L = \sum_{k=1}^{N} l_k$$
Step. 3: Calculate the average load. $$\bar{L} = \frac{1}{N} \sum_{k=1}^{N} l_k$$
Step. 4: Determine the *sender processor* and the *receiver processor*. $$if \begin{cases} l_k > \bar{L} & \Rightarrow \quad sender\ \ processor \\ l_k < \bar{L} & \Rightarrow \quad receiver\ \ processor \end{cases} \qquad k = 1, 2, \ldots, N$$
Step. 5: $sender\ \ processors \xrightarrow{load} receiver\ \ processors$
Step. 6: Solve the reaction stiff ODEs.
Step. 7: $sender\ \ processors \xleftarrow{updated\ \ values} receiver\ \ processors$

3. Validation tests

Compressible reactive flow and detonation can be simulated using detonationFoam in which both AMR and DLB are used. In this section, typical tests for

0D/1D/2D non-reactive/reactive problems are conducted to evaluate the capability and accuracy of detonationFoam. Moreover, the computational efficiency improved by AMR and DLB is assessed.

3.1 Homogeneous ignition process (0D)

Homogeneous ignition processes under constant volume conditions for different fuel/air mixtures are simulated to assess the performance of detonationFoam in terms of simulating chemical reactions. Stoichiometric H_2/air and n-heptane/air mixtures, respectively without and with negative temperature coefficient phenomenon [49], are considered. The detailed kinetic model for hydrogen and n-heptane are respectively from Li et al. [50] and Liu et al. [51]. The ignition delay time at different initial temperatures (1000 K < T_0 < 1300 K for H_2/air mixture and 700 K < T_0 < 1300 K for n-heptane/air mixture) and different initial pressures (P_0 = 0.1, 0.5 and 1 atm for H_2/air mixture and P_0 = 10, 20 and 30 atm for n-heptane/air mixture) are calculated and the results are plotted in Fig. 3. It is seen that good agreement between the results predicted by detonationFoam and by Cantera [41] (the maximum of the relative difference is lower than 7%). This demonstrates that the stiff ODE solver, *seulex*, used in detonationFoam can accurately simulate the homogeneous ignition process and thereby can be used to deal with chemical reactions.

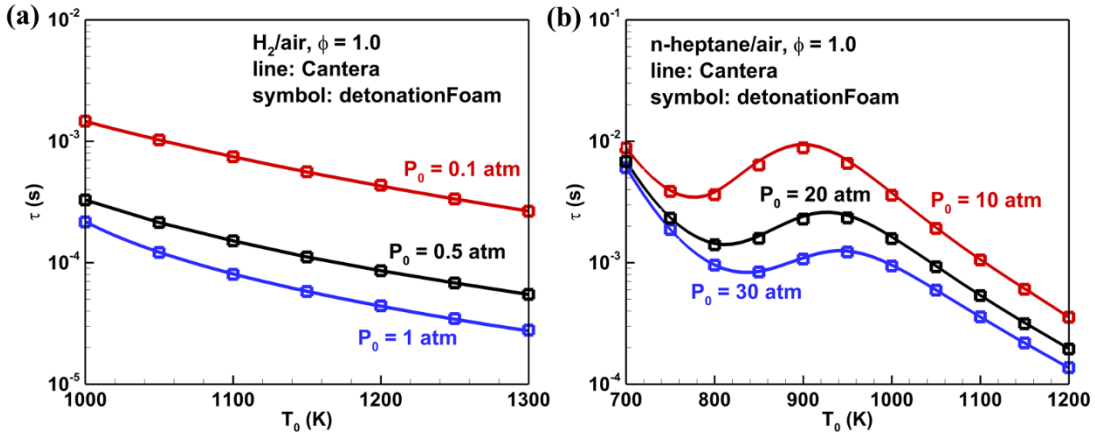

Fig. 3. Change of the ignition delay time with initial temperature at different pressures for stoichiometric (a) H_2/air and (b) n-heptane/air mixtures.

3.2 Unsteady diffusion process (1D)

Then, the 1D unsteady diffusion process is simulated to evaluate the reliability of the transport model and the numerical treatment of diffusion term in detonationFoam. We consider a static mixture in which there is a jump in the temperature and mixture composition across x = 1 cm. The initial conditions are:

$$\left(\mathrm{P,\ T,\ u,\ Y_{H_2}, Y_{N_2}}\right)=\begin{cases}\left(1\ \mathrm{atm},\ 300\ \mathrm{K},\ 0,\ 0.3,\ 0.7\right) & \mathrm{x < 1\ cm}\\ \left(1\ \mathrm{atm},\ 1500\ \mathrm{K},\ 0,\ 0.7,\ 0.3\right) & \mathrm{x > 1\ cm}\end{cases} \tag{27}$$

Note the Soret effects of H_2 is considered in this case. Uniform cell with the size of Δx = 20 μm is used. Transmissive boundary conditions are used at both x = 0 cm and x = 2 cm. Figure 4 shows the distributions of mass fraction of N_2 and temperature at t = 1 ms and t = 2 ms predicted by detonationFoam and A-SURF [52]. Very good agreement is achieved, which demonstrates that detonationFoam can accurately resolve the diffusion processes including both heat conduction and mass diffusion respectively due to temperature and concentration gradients.

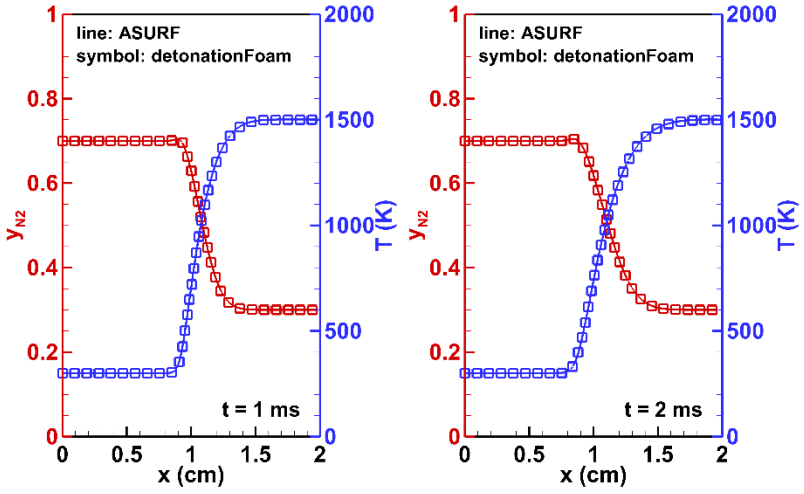

Fig. 4. The distributions for mass fraction of N_2 and temperature predicted by A-SURF (lines) and detonationFoam (symbols) at (a) t = 1 ms and (b) t = 2 ms.

3.3 The shock tube problem (1D)

The 1D shock tube problem is popularly used to assess the performance of numerical evaluation of convective fluxes for compressible flows [53]. We consider a jump in pressure and temperature across x = 0 cm. The initial conditions are given as:

$$(\mathrm{P},\ \mathrm{T},\ \mathrm{u}) = \begin{cases} (100\ \mathrm{kPa},\ 348.4\ \mathrm{K},\ 0) & \mathrm{x} < 0\ \mathrm{cm} \\ (10\ \mathrm{kPa},\ 278.7\ \mathrm{K},\ 0) & \mathrm{x} > 0\ \mathrm{cm} \end{cases} \tag{28}$$

Uniform cell with the size of $\Delta x = 20$ μm is also used and the transmissive boundary conditions are set for both ends of the computational domain. The pressure and density distributions predicted by detonationFoam at t = 50 μs are compared with the exact solutions [54] in Fig. 5(a). The maximum relative error for pressure is 1.78%, which indicates that detonationFoam can accurately simulate the shock tube problem. Figure 5(b) compares the results across the shock wave predicted by KNP [24], HLLC [28] and HLLC-P [36] schemes. It is seen that compared to KNP and HLLC schemes, HLLC-P used in detonationFoam has lower dissipation and thereby can more accurately resolve the shock propagation.

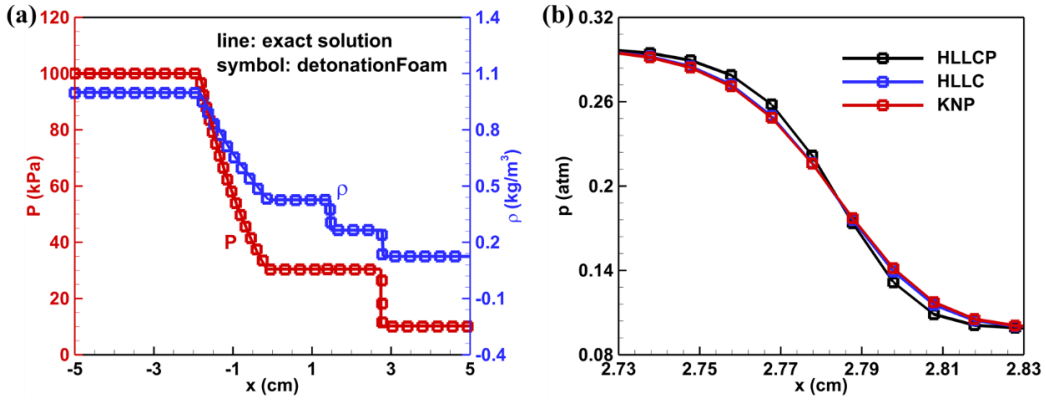

Fig. 5. (a) The pressure and density distributions at t = 50 μs and (b) the shock wave resolved by different schemes.

3.4 Laminar premixed planar flame (1D)

In the above three sub-sections, chemical reaction and transport/flow are decoupled. Here we use detonationFoam to simulate 1D premixed flame propagation, in which chemistry and transport are intrinsically coupled. We consider H_2/air mixtures at normal temperature and pressure, i.e., T_u = 300 K and P = 1 atm. The laminar flame speeds obtained from simulations using detonationFoam are compared to those predicted by Cantera [41] in Fig. 6. The relative difference is within 4%. Furthermore, the flame structure (i.e., distributions of temperature, total heat release rate, flow velocity, and mass fraction of OH) predicted by detonationFoam is also compared to

that predicted by Cantera [41]. Figure 7 shows that satisfactory agreement is achieved, which demonstrates that detonation is able to simulate premixed flame propagation. Therefore, detonation can be used to simulate the detonation initiation, quenching and reinitiation processes [55, 56], in which flame acceleration and deflagration-to-detonation transition might occur.

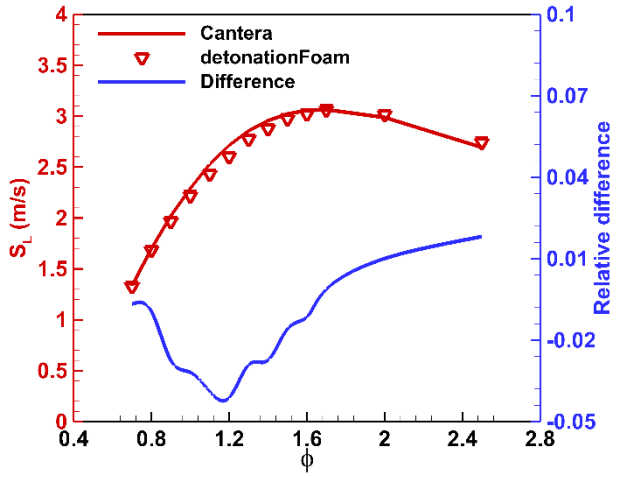

Fig. 6 Change of the laminar flame speed and relative difference with the equivalence ratio for H_2/air mixtures at T_u = 300 K and P = 1 atm.

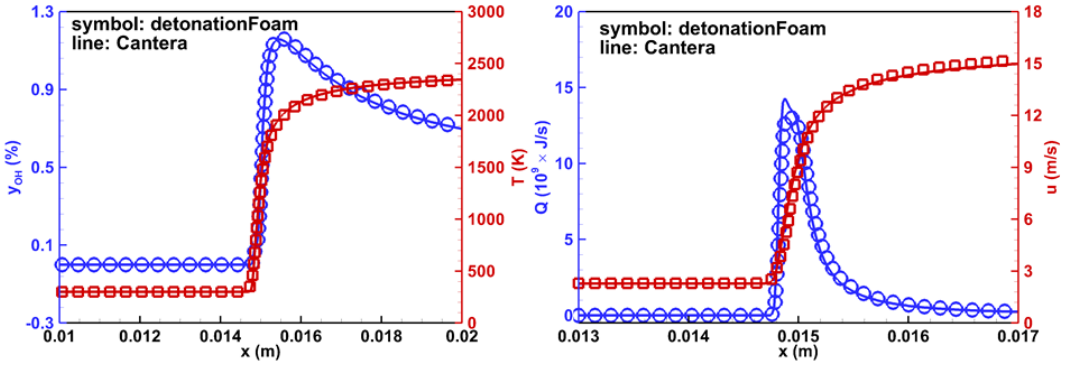

Fig. 7 The distributions for mass fraction of OH, temperature, total heat release rate and flow velocity of 1D premixed planar flame in a stoichiometric H_2/air mixture at T_u = 300 K and P = 1 atm.

3.5 Planar steady detonation propagation (1D)

Besides the flame/deflagration considered in the previous subsection, we also consider 1D planar detonation propagation process in a stoichiometric H_2/air mixture. The static mixture is initially at T_0 = 300 K and P_0 = 1 atm. A high-pressure hot spot

with T = 3000 K and P = 90 atm in the region of $0 < x < 2$ mm is used to initiate the detonation propagation. The uniform cell size of Δx = 20 μm is used. As shown in Fig. 8, the temporal evolution of pressure and O_2 mass fraction distributions predicted by detonationFoam and A-SURF are almost identical. Moreover, Fig. 8(a) shows that the peak pressure immediately after the leading shock is almost the same as the Von Neumann pressure, P_{VN} = 27.7 atm predicted by Chapman-Jouguet (C-J) theory. The detonation propagation speed predicted by detonationFoam is 2026 m/s, which is slightly higher but very close to the CJ value of V_{CJ} = 1977 m/s. Therefore, detonationFoam can accurately simulate 1D detonation propagation.

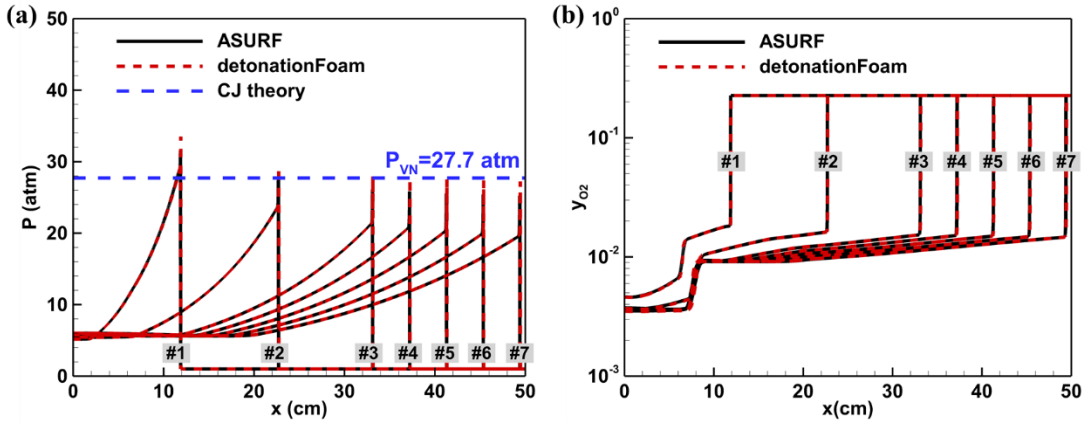

Fig. 8 Temporal evolution of (a) pressure and (b) O_2 mass fraction distributions predicted by detonationFoam (dashed red lines) and A-SURF (solid black lines) for 1D detonation propagation in a stoichiometric H_2/air mixture at T_0 = 300 K and P_0 = 1 atm. The time sequence is #1: 50 μs, #2: 100 μs, #3: 150 μs, #4: 170 μs, #5: 190 μs, #6: 210 μs, and #7: 230 μs.

3.6 Pulsating detonation wave (1D)

Referring to Sun et al.'s work [57], the pulsating detonation propagation process in $C_2H_4/O_2/Ar$ mixture is simulated and the initial fields are set as

$$(\mathrm{P,\ T,\ u}) = \begin{cases} (22.5\ \mathrm{atm},\ 2500\ \mathrm{K},\ 0\ \mathrm{m/s}) & \mathrm{x} < 0.2\ \mathrm{cm} \\ (0.25\ \mathrm{atm},\ 300\ \mathrm{K},\ 0\ \mathrm{m/s}) & \mathrm{x} > 0.2\ \mathrm{cm} \end{cases} \tag{29}$$

Then detonationFoam is employed to simulate the process and the results are presented in Fig. 9. Figure 9(a) shows the pressure curve peaks cyclically oscillate when

the detonation wave propagates into the region of $x > 0.75$ cm. Figure 9(b) records the leading shock speed, U_S, as a function of its position, x_S. It shows the detonation wave propagation speed oscillates periodically around the C-J speed (U_{CJ}) and the oscillation period and amplitude almost remain constant when $x_S > 0.15$ m. The pulsating period obtained by detonationFoam is 9.93 μs and closed to the reference value, 6.32 μs, predicted by Sun et al. [57].

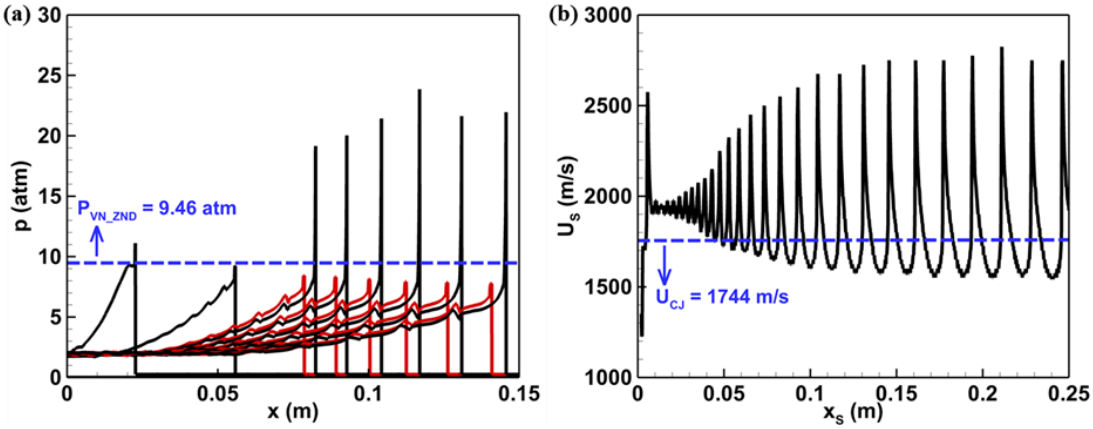

Fig. 9 (a) Temporal pressure distribution curves and (b) leading shock speed as a function of its position during the pulsating detonation propagation process in $C_2H_4/O_2/Ar$ mixture. X_{C2H4}: X_{O2}: X_{Ar} = 1:3:7, T_0 = 300 K and P_0 = 0.25 atm.

3.7 Double Mach reflection (2D)

Following the work of Woodward and Colella [58, 59], we simulate the well-known double Mach reflection problem to assess numerical accuracy and robustness under high-Mach conditions. A normalized inviscid gas model is used for simulation purposes only. The heat capacity ratio is 1.4. An incident shock wave with Mach number of 10 reflects on a wall oriented at an angle of 60º. The density contour at t = 0.2 s are shown in Fig. 10(a), which is almost consistent with the result predicted by Woodward et al. [58] shown in Fig. 10(b). AMR with cell level from 0 (coarsest) to 4 (finest) is used. The cell distribution and level are shown in Figs. 10(c-d). It is observed that the shock waves and contact discontinuities are covered by the finest cells. Therefore, AMR incorporated in detonationFoam helps to efficiently resolve the different waves in compressible flow.

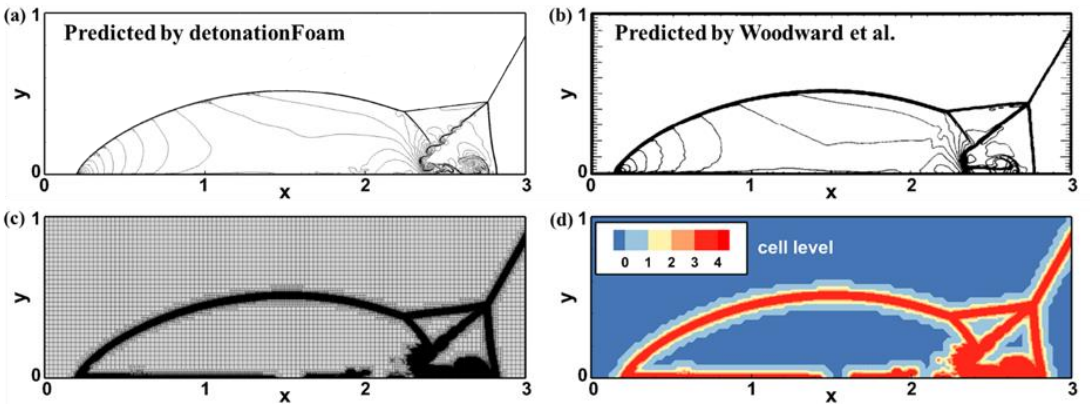

Fig. 10 The density contours separately predicted by (a) detonationFoam and (b) Woodward et al. [58], (c) cell distribution and (d) cell level distribution for the 2D double Mach reflection problem.

3.8 Cellular structure of planar detonation propagation (2D)

As an important characteristic of detonation, its cellular structure should be simulated. Following the work of Oran et al. [60], we simulate the detonation propagation process in a $H_2/O_2/Ar$ mixture and schematic of the computational domain and the initial conditions are shown in Fig. 11(a). The triple point trajectories predicted by detonationFoam and Oran et al. [60] are recorded and separately plotted in Figs. 11(b-c). As results, we predicte a cell size of approximately 55 × 30 mm using detonationFoam which is closed to previously reported values (54 ×31 mm by Oran et al. [60] and 54×30 mm by Wang et al. [61], respectively).

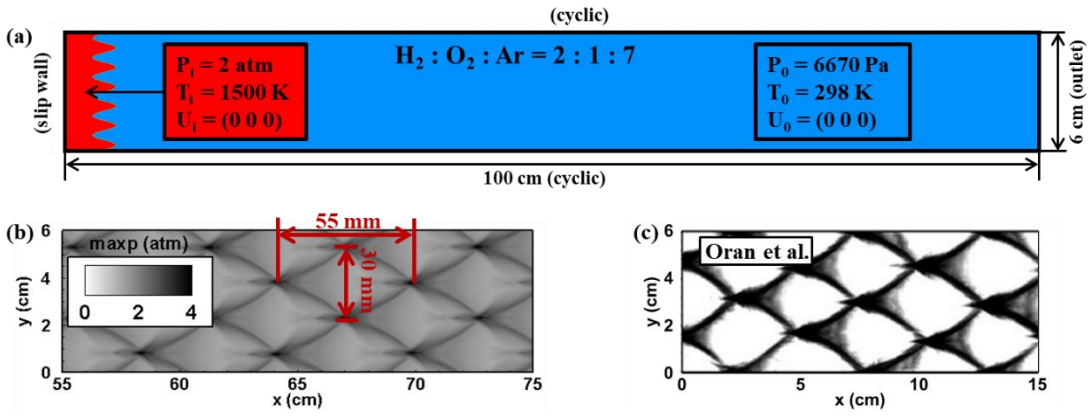

Fig. 11 (a) Schematic of the computational domain and the initial and boundary conditions; (b) triple-wave point trajectories predicted by detonationFoam; and (c) soot foils of triple-wave point trajectories reported by Oran et al. [60].

The induction length for the $H_2/O_2/Ar$ mixture at T_0 = 300 K and P_0 = 6670 Pa predicted by SDtoolbox [62] equals to 1519 μm. In the above case, uniform cells with $\Delta x = \Delta y$ = 200 μm are used as basic cells and three-level adaptive refinement cells are adopted. Thereby the finest cell size is $200/2^3$ = 25 μm, which ensures that there are more than 60 cells resolving the induction region. Figure 12 shows the temperature, pressure, density gradient and cell level at t = 532 μs. It is seen that the cellular structure of the propagating detonation can be simulated efficiently using AMR in detonationFoam.

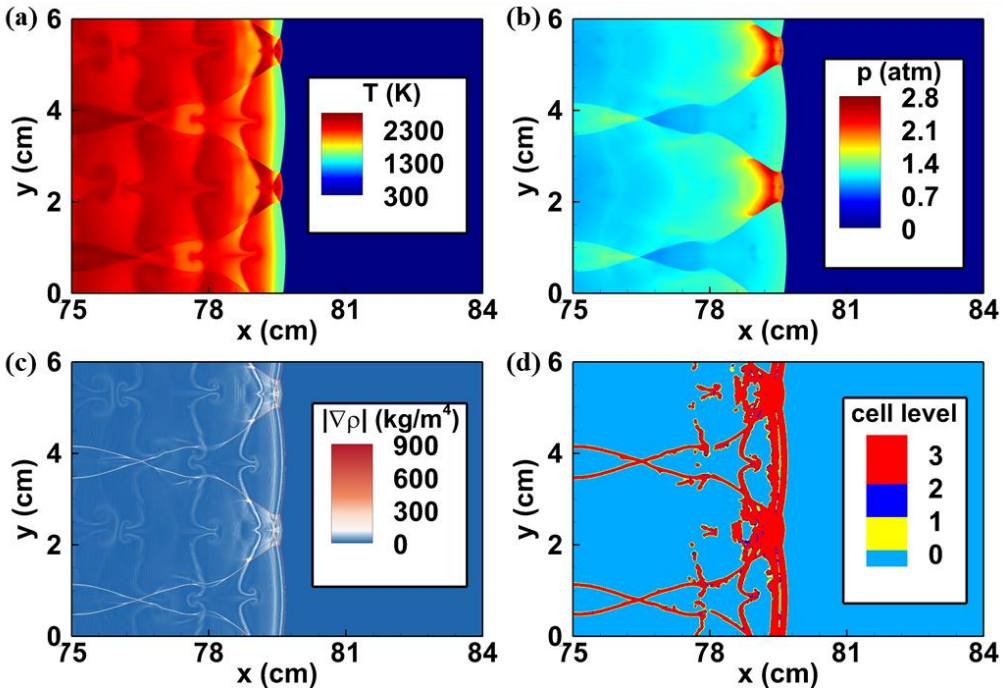

Fig. 12 The contours for (a) temperature, (b) pressure, (c) absolute value of density gradient and (d) cell level at t = 532 μs for detonation propagation in a stoichiometric $H_2/O_2/Ar$ mixture at T_0 = 300 K and P_0 = 6670 Pa predicted by detonationFoam.

3.9 The oblique detonation wave (2D)

Finally, the wedge-stabilized oblique detonation wave in a stoichiometric H_2/air

mixture is simulated using detonationFoam and compared with the results of Teng et al. [63]. Additionally, the computing efficiency improved by AMR and DLB algorithms is also evaluated.

The computational domain is similar to previous studies [64-66] and is schematically described in Fig. 13. The wedge starts from $x = y = 0$ cm. The inflow states are specified as P_0 = 196.3 kPa, T_0 = 814.4 K, and V_0 = 2418.9 m/s, which are calculated based on the specified flight altitude, H_0 = 20 km, and flight Mach number, Ma_0 = 9, according to Teng et al. [63]. The base cell size (i.e., the cell level is zero) is $\Delta x = \Delta y$ = 20 μm and the maximum cell level is 2 during the AMR. In fact, detonationFoam has been successfully used in oblique detonation simulation. The corresponding grid and time dependency tests were conducted and shown in Fig. 2 of the reference [66]. The results indicate cell size of 5 μm can ensure that the oblique detonation wave can be adequately resolved in such an operating condition for H_2/air mixture. Note that the diffusion terms are ignored in the conservation equations and thereby Euler equations are solved. The steady oblique detonation wave structures predicted by detonationFoam and Teng et al. [63] are shown in Fig. 14. Almost identical oblique detonation wave structures are acquired and the ability of detonationFoam in detonation simulations is verified further.

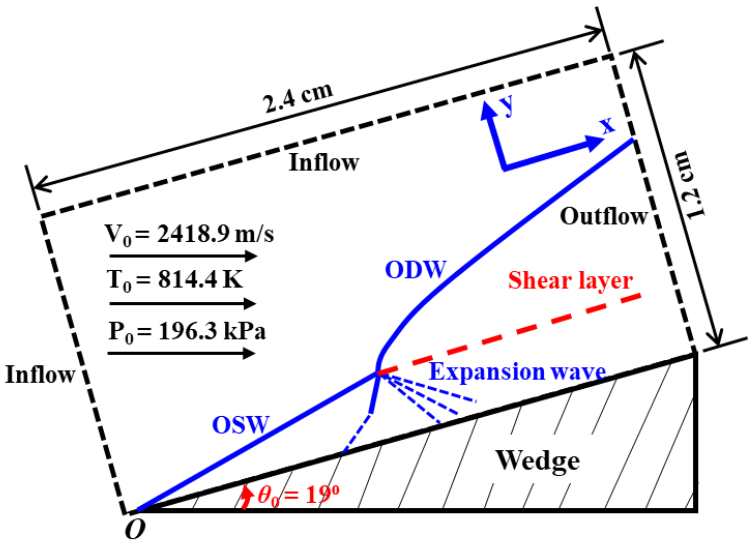

Fig. 13 Schematic of the initial and boundary conditions for the 2D wedge-stabilized oblique detonation wave in a stoichiometric H_2/air mixture. ODW: oblique detonation wave; OSW: oblique shock wave.

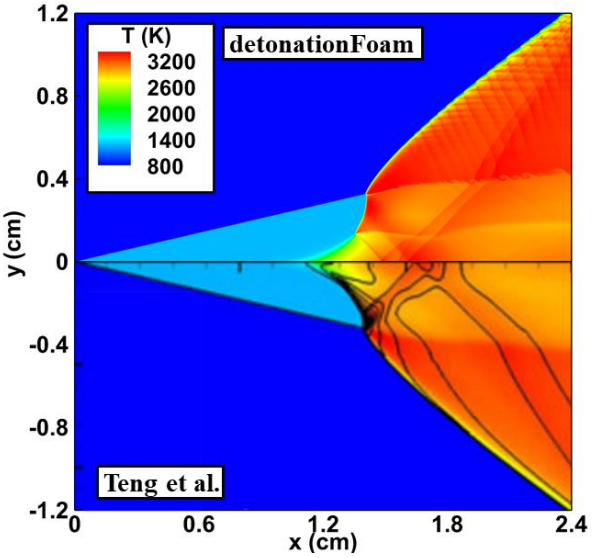

Fig. 14 The steady temperature distribution for the wedge-stabilized oblique detonation wave in a stoichiometric H_2/air mixture. The results predicted by detonationFoam (up) and Teng et al. [63] (down) are shown together for comparison.

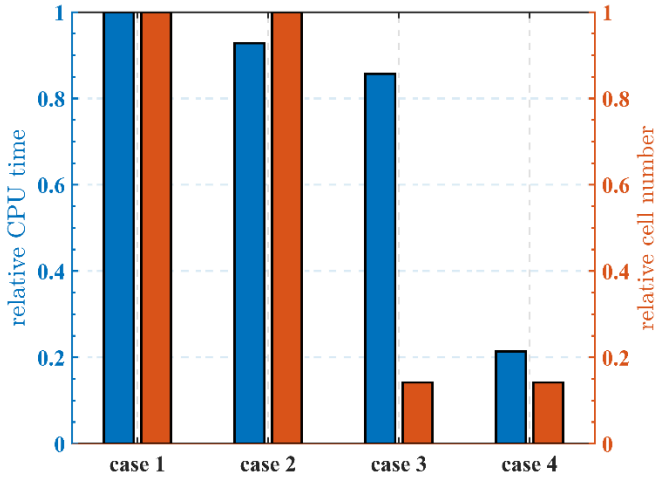

Fig. 15 The relative CPU time and cell number for cases 1-4 of the steady wedge-stabilized oblique detonation wave in a stoichiometric H_2/air mixture.

To evaluate the computational efficiency improved by AMR and DLB algorithms

used in detonationFoam, we compare the cell number and computational time for the simulation of the wedge-stabilized oblique detonation wave under four cases: uniform mesh without DLB (case 1), uniform mesh with DLB (case 2), adaptive mesh without DLB (case 3) and adaptive mesh with DLB (case 4). It is noted that the finest cell size in case 2 and case 4 is the same. The normalized cell number and the CPU time for these four cases are plotted in Fig. 15. Compared with case 1 using uniform mesh and without DLB, in case 3 the cell number is reduced to about 1/6 by using AMR and the CPU time is reduced to about 1/5 by using AMR and DLB. This demonstrates that high computing efficiency can be achieved by using the AMR and DLB in detonationFoam. Besides, the steady ODW structure for cases 1-4 (see Fig. 16) are almost same, indicating that AMR and DLB have little influence on the accuracy of simulation results.

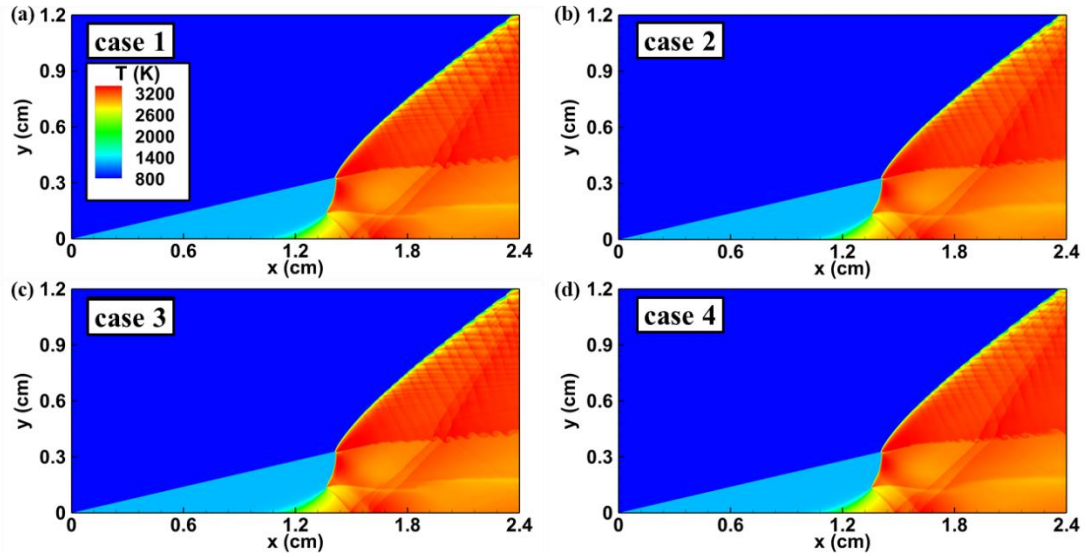

Fig. 16 The steady temperature distribution for the wedge-stabilized oblique detonation wave in a stoichiometric H_2/air mixture separately for cases 1-4.

4. Conclusions

In this work, we develop an OpenFOAM-based open-source solver, detonationFoam, which can accurately and efficiently simulate gaseous detonation. The solver is developed based on rhoCentralFoam, and five major improvements are made. First, the species equations and detailed finite-rate chemistry are considered and thereby the compressible, multi-component, reactive flow can be simulated. Second, the

mixture-averaged transport model is used and it can accurately evaluate the detailed transport coefficients. Third, the improved HLLC-P approximate Riemann solver is used and it has advantages in accurately capturing the propagation of shock wave and contact discontinuity. Fourth, the two-dimensional adaptive mesh refinement (AMR) technique is incorporated into the solver so that the detonation front can be resolved by the finest meshes. Fifth, the dynamic load balancing (DLB) algorithm is used to further improve the computational efficiency.

Comprehensive validation tests for both non-reactive and reactive flows have been conducted. These tests demonstrate that detonationFoam can accurately and efficiently simulate compressible, multi-component reactive flow and detonation processes. The computational efficiency can be greatly improved by using AMR and DLB algorithms simultaneously incorporated into detonationFoam.

Acknowledgement

This work was supported by National Natural Science Foundation of China (No. 52176096). We also thank Professor Huangwei Zhang at National University of Singaporeand Professor Tianhan Zhang at Southern University of Science and Technology for helpful discussion. The computations for this article were supported on resources of the Dawning Information Industry Co., Ltd., China (https://ac.sugon.com).

References

[1] B.A. Rankin, M.L. Fotia, A.G. Naples, C.A. Stevens, J.L. Hoke, T.A. Kaemming, S.W. Theuerkauf, F.R. Schauer, Overview of performance, application, and analysis of rotating detonation engine technologies, Journal of Propulsion and Power 33 (2017) 131-143.

[2] G.D. Roy, S.M. Frolov, A.A. Borisov, D.W. Netzer, Pulse detonation propulsion: challenges, current status, and future perspective, Progress in Energy and Combustion Science 30 (2004) 545-672.

[3] P. Wolański, Detonative propulsion, Proceedings of the Combustion Institute 34 (2013) 125-158.

[4] Q. Xie, Z. Ji, H. Wen, Z. Ren, P. Wolanski, B. Wang, Review on the rotating detonation engine and it's typical problems, Transactions on Aerospace Research 2020 (2020) 107-163.

[5] R. Zhou, D. Wu, J. Wang, Progress of continuously rotating detonation engines, Chinese Journal of Aeronautics 29 (2016) 15-29.
[6] J.E. Shepherd, Detonation in gases, Proceedings of the Combustion Institute 32 (2009) 83-98.
[7] D.A. Schwer, R.F. Johnson, A. Kercher, D. Kessler, A.T. Corrigan, Progress in efficient, high-fidelity, rotating detonation engine simulations, AIAA Scitech 2019 Forum, 2019.
[8] J.M. Powers, Review of multiscale modeling of detonation, Journal of Propulsion and Power 22 (2006) 1217-1229.
[9] E.S. Oran, V.N. Gamezo, Origins of the deflagration-to-detonation transition in gas-phase combustion, Combustion and Flame 148 (2007) 4–47.
[10] J.Z. Ma, M.-Y. Luan, Z.-J. Xia, J.-P. Wang, S.-j. Zhang, S.-b. Yao, B. Wang, Recent progress, development trends, and consideration of continuous detonation engines, AIAA Journal 58 (2020) 4976-5035.
[11] OpenFOAM, https://openfoam.org/.
[12] A. López, W. Nicholls, M.T. Stickland, W.M. Dempster, CFD study of jet impingement test erosion using Ansys Fluent® and OpenFOAM®, Computer Physics Communications 197 (2015) 88-95.
[13] P. Horgue, C. Soulaine, J. Franc, R. Guibert, G. Debenest, An open-source toolbox for multiphase flow in porous media, Computer Physics Communications 187 (2015) 217-226.
[14] Q. Meng, N. Zhao, H. Zhang, On the distributions of fuel droplets and in situ vapor in rotating detonation combustion with prevaporized n-heptane sprays, Physics of Fluids 33 (2021) 043307.
[15] T. Zirwes, F. Zhang, P. Habisreuther, M. Hansinger, H. Bockhorn, M. Pfitzner, D. Trimis, Quasi-DNS dataset of a piloted flame with inhomogeneous inlet conditions, Flow, Turbulence and Combustion 104 (2019) 997-1027.
[16] A. Dasgupta, E. Gonzalez-Juez, D.C. Haworth, Flame simulations with an open-source code, Computer Physics Communications 237 (2019) 219-229.
[17] Q. Yang, P. Zhao, H. Ge, reactingFoam-SCI: An open source CFD platform for reacting flow simulation, Computers & Fluids 190 (2019) 114-127.
[18] D. Zhou, H. Zhang, S. Yang, A robust reacting flow solver with computational diagnostics based on OpenFOAM and Cantera, Aerospace 9 (2022) 102-119.
[19] C.K. Law, Combustion physics, Cambridge University Press, 2010.
[20] V. Giovangigli, Multicomponent transport in laminar flames, Proceedings of the Combustion Institute 35 (2015) 625-637.
[21] S.D. Cohen, A.C. Hindmarsh, P.F. Dubois, CVODE, a stiff/nonstiff ODE solver in C, Computers in Physics 10 (1996) 138-143.
[22] J.H.S. Lee, The detonation phenomenon, Cambridge University Press, 2008.
[23] A. Kurganov, E. Tadmor, New high-resolution central schemes for nonlinear conservation laws and convection–diffusion equations, Journal of Computational Physics 160 (2000) 241-282.
[24] A. Kurganov, S. Noelle, A. Petrova, Semidiscrete central-upwind schemes for hyperbolic conservation laws and Hamilton-Jacobi equations, SIAM Journal on

Scientific Computing 23 (2001) 707-740.
[25] L.F. Gutiérrez Marcantoni, J. Tamagno, S. Elaskar, rhoCentralRfFoam: An OpenFOAM solver for high speed chemically active flows – simulation of planar detonations –, Computer Physics Communications 219 (2017) 209-222.
[26] X.-Y. Liu, M.-Y. Luan, Y.-L. Chen, J.-P. Wang, Flow-field analysis and pressure gain estimation of a rotating detonation engine with banded distribution of reactants, International Journal of Hydrogen Energy 45 (2020) 19976-19988.
[27] Z. Huang, M. Zhao, Y. Xu, G. Li, H. Zhang, Eulerian-Lagrangian modelling of detonative combustion in two-phase gas-droplet mixtures with OpenFOAM: Validations and verifications, Fuel 286 (2021) 119402.
[28] E.F. Toro, M. Spruce, W. Speares, Restoration of the contact surface in the HLL-Riemann solver, Shock Waves 4 (1994) 25-34.
[29] H. Guo, Y. Xu, S. Li, H. Zhang, On the evolutions of induction zone structure in wedge-stabilized oblique detonation with water mist flows, Combustion and Flame 241 (2022) 112122.
[30] Y. Xu, H. Zhang, Pulsating propagation and extinction of hydrogen detonations in ultrafine water sprays, Combustion and Flame 241 (2022) 112086.
[31] A. Baniabedalruhman, Dynamic meshing around fluid-fluid interfaces with applications to droplet tracking in contraction geometris, Michigan Technological University, 2015.
[32] D. Rettenmaier, D. Deising, Y. Ouedraogo, E. Gjonaj, H. De Gersem, D. Bothe, C. Tropea, H. Marschall, Load balanced 2D and 3D adaptive mesh refinement in OpenFOAM, SoftwareX 10 (2019) 100317.
[33] B. Tekgül, P. Peltonen, H. Kahila, O. Kaario, V. Vuorinen, DLBFoam: An open-source dynamic load balancing model for fast reacting flow simulations in OpenFOAM, Computer Physics Communications 267 (2021) 108073.
[34] T. Zirwes, F. Zhang, P. Habisreuther, J.A. Denev, H. Bockhorn, D. Trimis, Implementation and validation of a computationally efficient DNS solver for reacting flows in OpenFOAM, 14th World Congress on Computational Mechanics, 2021.
[35] D.A. McGough, Detonation modeling in OpenFOAM using adaptive mesh refinement, University of Colorado Boulder, 2020.
[36] W. Xie, R. Zhang, J. Lai, H. Li, An accurate and robust HLLC-type Riemann solver for the compressible Euler system at various Mach numbers, International Journal for Numerical Methods in Fluids 89 (2018) 430-463.
[37] blastFoam: An OpenFOAM solver for compressible multi-fluid flow with application to high-explosive detonation, Synthetik Applied Technologies, LLC., 2019.
[38] P.J. Vonk, M. Safdari, M.D. Brandyberry, A new OpenFOAM solver for compressible multi-fluid flow with application to high-explosive detonation, the 4th OpenFOAM User Conference 2016, Germany, 2016.
[39] T. Poinsot, D. Veynante, Theoretical and numerical combustion, R.T. Edwards, Inc., 2005.
[40] D.R. Stull, H. Prophet, JANAF thermochemical tables, second ed., U.S. National Bureau of Standards, 1971.
[41] Cantera, https://cantera.org/.

[42] R.B. Bird, W.E. Stewart, E.N. Lightfoot, Transport Phenomena, second ed., John Wiley & Sons, Inc., 2006.
[43] C.R. Wilke, A viscosity equation for gas mixtures, The Journal of Chemical Physics 18 (1950) 517-519.
[44] S. Mathur, P.K. Tondon, S.C. Saxena, Thermal conductivity of binary, ternary and quaternary mixtures of rare gases, Molecular Physics 12 (1967) 569-579.
[45] R.J. Kee, F.M. Rupley, J.A. Miller, M.E. Coltrin, J.F. Grcar, E. Meeks, H.K. Moffat, A.E. Lutz, G. Dixon-Lewis, M.D. Smooke, J. Warnatz, G.H. Evans, R.S. Larson, R.E. Mitchell, L.R. Petzold, W.C. Reynolds, M. Caracotsios, W.E. Stewart, P. Glarborg, C. Wang, O. Adigun, TRANSPORT-a software package for the evaluation of gas-phase, multicomponent transport properties, Reaction Design, Inc., 2000.
[46] M.Y. Hussaini, B.v. Leer, J.V. Rosendale, Upwind and high-Resolution schemes, first ed., Springer Berlin, Heidelberg1997.
[47] E. Hairer, S.P. Nørsett, G. Wanner, Solving Ordinary Differential Equations II: Stiff and Differential-Algebraic Problems, second ed., Springer-Verlag, Berlin, 1996.
[48] W. Xie, W. Li, H. Li, Z. Tian, S. Pan, On numerical instabilities of Godunov-type schemes for strong shocks, Journal of Computational Physics 350 (2017) 607-637.
[49] X. Fu, S.K. Aggarwal, Two-stage ignition and NTC phenomenon in diesel engines, Fuel 144 (2015) 188-196.
[50] J. Li, Z. Zhao, A. Kazakov, M. Chaos, F.L. Dryer, J.J. Scire, A comprehensive kinetic mechanism for CO, CH2O, and CH3OH combustion, International Journal of Chemical Kinetics 39 (2007) 109-136.
[51] S. Liu, J.C. Hewson, J.H. Chen, H. Pitsch, Effects of strain rate on high-pressure nonpremixed n-heptane autoignition in counterflow, Combustion and Flame 137 (2004) 320-339.
[52] Z. Chen, Studies on the initiation, propagation, and extinction of premixed flames, Princeton University, 2009.
[53] E.F. Toro, Riemann solvers and numerical methods for fluid dynamics (Third Edition), Springer, 2009.
[54] J.M. Martí, E. Müller, The analytical solution of the Riemann problem in relativistic hydrodynamics, Journal of Fluid Mechanics 258 (2006) 317-333.
[55] Y. Wang, W. Han, R. Deiterding, Z. Chen, Effects of disturbance on detonation initiation in H2/O2/N2 mixture, Physical Review Fluids 3 (2018) 123201.
[56] Y. Wang, C. Huang, R. Deiterding, H. Chen, Z. Chen, Propagation of gaseous detonation across inert layers, Proceedings of the Combustion Institute 38 (2021) 3555-3563.
[57] J. Sun, B. Tian, Z. Chen, Effect of ozone addition and ozonolysis reaction on the detonation properties of C2H4/O2/Ar mixtures, Proceedings of the Combustion Institute 39 (2023) 2797-2806.
[58] P.C. P. Woodward, The numerical simulation of two-dimensional fluid flow with strong shocks, Journal of Computational Physics 54 (1984) 115-173.
[59] U.S. Vevek, B. Zang, T.H. New, On Alternative Setups of the Double Mach Reflection Problem, Journal of Scientific Computing 78 (2018) 1291-1303.
[60] E.S. Oran, J.W.W. Jr., E.I. Stefaniw, M.H. Lefebvre, J.D.A. Jr., A numerical study

of a two-dimensional H2-O2-Ar detonation using a detailed chemical reaction model, Combustion and Flame 113 (1998) 147-163.
[61] C.J. Wang, S.L. Xu, C.M. Guo, Gaseous detonation propagation in a bifurcated tube, Journal of Fluid Mechanics 599 (2008) 81-110.
[62] S. Browne, J. Ziegler, J.E. Shepherd, https://shepherd.caltech.edu/EDL/PublicResources.
[63] H. Teng, C. Tian, Y. Zhang, L. Zhou, H.D. Ng, Morphology of oblique detonation waves in a stoichiometric hydrogen–air mixture, Journal of Fluid Mechanics 913 (2021) A1.
[64] P. Yang, H.D. Ng, H. Teng, Numerical study of wedge-induced oblique detonations in unsteady flow, Journal of Fluid Mechanics 876 (2019) 264-287.
[65] P. Yang, H.D. Ng, H. Teng, Unsteady dynamics of wedge-induced oblique detonations under periodic inflows, Physics of Fluids 33 (2021) 016107.
[66] J. Sun, P. Yang, B. Tian, Z. Chen, Effects of wedge-angle change on the evolution of oblique detonation wave structure, Physics of Fluids 34 (2022) 096112.